A novel thermal management system for battery packs in hybrid electrical vehicles utilising waste heat recovery

Hengrui Liu [a,1], Chuang Wen [b,1], Anthony Chun Yin Yuen [a]*, Yu Han [c, d], Sherman Chi-Pok Cheung [e], Sanghoon Kook [a] and Guan Heng Yeoh [a, f]

[a] School of Mechanical and Manufacturing Engineering, University of New South Wales, Sydney, NSW 2052, Australia
[b] College of Engineering, Mathematics and Physical Sciences, University of Exeter, North Park Road, Exeter EX4 4QF, United Kingdom
[c] School of Mechanical and Electrical Engineering, Suqian University, Jiangsu, P.R. China
[d] School of Mechanical Engineering and Automation, Northeastern University, Shenyang, P.R. China
[e] School of Mechanical and Automotive Engineering, RMIT University, Melbourne, VIC 3000, Australia
[f] Australian Nuclear Science and Technology Organization (ANSTO), Locked Bag 2001, Kirrawee DC, NSW 2232, Australia

***** Correspondence: c.y.yuen@unsw.edu.au; Tel.: +61-2-9385 5697

Abstract: Thermal management system generally ensures the safe operating conditions and heat resilience of battery packs in hybrid electric vehicles (HEVs). The current study raised a novel approach to reduce fire risks related to HEVs through a novel battery thermal management system powered by low-grade combustion waste heat running on steam ejectors for the first time. In this paper, an ejector operating at a low temperature under 100° C for HEV's battery thermal management system is proposed and investigated. An in-house wet-steam model considering the condensation effect has been developed to characterise the ejector's internal flow structure and further analyse its feasibility as a thermal management system. The results show that the model considering the condensation process is more feasible in evaluating the performance of the steam ejector than the dry gas assumption. To improve the performance of the proposed ejector battery thermal management system, the effect of superheating of primary steam has been investigated. The results showed that an optimum point exists with 11 K superheating between improvement of entrainment ratio, the system's coefficient of performance and the power efficiency for the current case. The entrainment ratio at that point reaches around 0.45, while the coefficient of performance reaches 0.225.

Keywords: Thermal Management; Low-grade Energy; Li-ion Battery; Fire Prevention; Hybrid Vehicles; Electric Vehicles

Nomenclature

Symbol	Physical meaning
E	Total energy
h_s, h_p, h_o	Enthalpy of secondary inlet, primary inlet and outlet
h_{lv}	Latent heat during phase change
J	Nucleation rate
k_B	Boltzmann's constant
$\dot{m}$	Condensation rate of vapour
$\dot{m}_s, \dot{m}_p$	Mass flow rate of the secondary inlet and primary inlet
m_v	Mass of one molecule
e	Exergy
p, p_{sat}	Pressure, Saturation pressure
q_c	Evaporation coefficient
r, r^*	Droplet radius, Critical droplet radius

1. Hengrui Liu and Chuang Wen contributed equally to this work.

R	Gas constant
s	Entropy
S	Supersaturation ratio
t	Time
T, T_d	Temperature, Temperature of a droplet
Y	Liquid mass fraction

Greek Symbols

Symbol	Physical meaning
$u_{i,j,k}$	Generic velocity
δ_{ij}	Kronecker delta
γ	Ratio of specific heat capacities
λ_{eff}	Effective thermal conductivity
μ_{eff}	Effective molecular dynamic viscosity
ν	Correction factor
ϕ	Non-isothermal correction factor
ρ, ρ_v, ρ_l	Density of mixture, Density of water vapour, Density of water droplets
τ_{ij}	Stress tensor
$x_{i,j,k}$	Generic position in space
$\boldsymbol{\psi_D}$	Exergy destruction ratio

Subscripts

Letter	Representing
0	Referencing point
s	Secondary inlet
p	Primary inlet
o	Outlet
lv	Phase change from liquid to vapour
sat	Saturation
d	Droplet
i, j, k	Velocity vector
eff	Effective
l	Liquid phase

Superscripts

Symbol	Representing
.	Rate of change

*	Critical (radius)

Abbreviation

Acronyms	Representing
HEV	Hybrid Electric Vehicle
EV	Electrical Vehicle
LIB	Li-ion Battery
PCM	Phase Change Materials
COP	Coefficient of Performance
CFD	Computational Fluid Dynamics
NXP	Nozzle Exit Position
X	Nozzle Exit Position
NEC	Non-Equilibrium Condensation
SST	Shear Stress Transport
PHEV	Plug-in Hybrid Electric Vehicle
HVAC	Heating, Ventilation and Air Conditioning
UDS	User-Defined Scalar
UDF	User-Defined Function
ER	Entrainment Ratio

1. Introduction

Due to global warming and other environmental concerns, green, renewable, and environmentally friendly energy sources have gained sustained attention from government authorities to mitigate carbon emissions. A case study on United Kindom also indicated that the increasing adoption of electrical vehicles (EVs) and hybrid electric vehicles (HEVs) will see a larger percentage of greenhouse gas reduction [1]. According to a recent review by Du and Ouyang on EVs [2], the huge marketing potential and policy support contributed significantly to the emergence and development of EVs and HEVs. Meanwhile, the increased usage of EV/HEVs also exposes us to more significant fire risks associated with Li-ion batteries (LIB) in new vehicles, which cannot be ignored [3]. Many EV fire incidents have been recorded in the recent decade, while most of these cases were initiated from the thermal runaway of their LIBs [4-6]. To ensure the safe and efficient use of LIBs, it is necessary to look into batterys' thermal behaviour during operation. To better understand the electrochemical thermal reactions happening inside the battery packs, Bizeray et al. developed an accurate physics-based cell model and applied orthogonal collocation to solve the thermal-electrochemical P2D model, the results showed good accuracy with less than 1% error [7]. Ma et al. developed an advanced model to couple the electrochemical-thermal effect for the state of charge estimation of lithium-ion batteries. The results showed that the model could effectively evaluate the state of charge [8]. Zhou, Li and Xie proposed a systematic fast-modelling approach to numerically investigate the thermal effect's impact on battery performances [9]. Furthermore, it was found that the EV/HEV fires were completely different scenarios from traditional vehicle fires since their fire risks were more predominantly related to combustible interiors such as polyurethane [10].

LIB fires are exceptionally hazardous as they are intense, rapid and complicated, involving toxic/acidic chemical compounds, making suppression of such fires extremely challenging [11]. To decrease the fire hazard and ensure a higher efficiency window for the battery packs, battery thermal management systems are crucial in EVs and HEVs. Currently, available working substances including air [12], liquid [13, 14], and even phase change materials (PCM) [15, 16], are being used as coolants for the battery packs. Although thermal management approaches have been investigated and implemented, the above-mentioned working substances were far from perfect. Air does not possess a large specific heat capacity, and liquid and phase change materials

are prone to leakage problems. Their self-weight will also bring an additional burden to the vehicles. More cost-effective methods are still desirable, especially in specific operating scenarios where the risk of a fire or explosion is high. Traditional thermal management systems usually operate on their own power supply, which requires additional energy from the main power source and another set of cooling apparatuses. To better integrate the battery thermal management systems with existing features well established in vehicles, Gan et al. proposed a novel heat pipe based system that can integrate with EV and HEV's refrigeration system to effectively utilise the spaces between cylindrical battery packs [17, 18]. However, similar to other refrigeration systems, the refrigeration systems in a vehicle usually use electrical energy as power sources, mainly to power the compressor.

Nonetheless, as a more energy efficient and environmentally friendly approach, ejector refrigeration systems were proposed for vehicles using internal combustion engines, where the ejector plays the same role as a compressor in the traditional refrigeration system. The beauty of steam ejector refrigeration systems is that they operate on the engine combustion waste heat as power input with simple structure, easy operation and high reliability. The combustion waste heat accounts for 30% of the total engine power and will be discharged to the ambient with exhaust gas if not recycled for other purposes [19]. The exhaust temperature from an internal combustion engine can reach 400°C to 700°C, which holds 2/3 of the combustion waste heat, while the rest 1/3 is discharged to engine coolant water at about 90°C. Various methods were examined and explored by researchers to recycle waste heat, and their effectiveness has also been validated [20, 21]. Zhang et al. [22] investigated waste heat recovery systems and obtained a net work of 33.06 kW and 58.7% recovery efficiency. Al-Nimr and Alajlouni [23] utilised a thermoelectric generator for recycling and obtaining 750 W electrical energy from engine waste heat. The combustion waste heat can be collected by utilising a steam ejector refrigeration system into HEVs and integrating it with the battery thermal management systems. The proposed thermal management system lowers the risk of battery pack thermal runaway and thus reduces the possibility of fire and explosion hazards caused by batteries.

Many numerical and experimental studies have been conducted previously to study the performances and efficiency of ejectors by analysing their entrainment ratio and coefficient of performance (COP). For instance, Yan et al. [24] conducted parametric studies for six key geometric parameters on the performance of an R134A ejector system using CFD simulation, and the results can serve as a reference when designing a new R134A ejector system. Selvaraju et al. [25] experimentally investigated an 0.5 kW R134A ejector system with a self-constructed small-scale ejector experiment rig with R134A. They utilised regression analysis to estimate the COP for the ejector. Water is also considered a promising working fluid for steam ejector systems, apart from studies using refrigerants. It possesses advantages such as being non-toxic, environmentally friendly, safe, and cheap. Therefore, many studies have been carried out for ejectors using water/water vapour. Bo et al. [26] utilised ejector systems to recover waste heat from exhaust gases from ship engines. They found that it is a cost-effective and clean production solution to improve the design of a ship. Dong et al. [27] experimentally investigated the effect of primary steam temperature and nozzle exit position (NXP) on a steam ejector. It was found that when the nozzle exit position is fixed, the ejector's COP is positively related to the diameter of the constant section. Han et al. studied the internal flow structure [28] and shock waves [29] inside a steam ejector powered by engine combustion waste heat. It was found that the internal flow structure, such as the pseudo-shock region and normal shock position, can affect the entrainment ratio. Thus a critical primary fluid pressure range is determined to optimise pumping efficiency. Wang et al. [30] investigated the potential for increasing the ejector's performace by increasing the superheating degree of primary flows. They suggested that the contribution of superheating is not as significant after 20K. Experimental and numerical studies from Zhang et al. [31] on superheated steam through IWSEP nozzle further confirmed the feasibility of studying condensing steam flows with superheating using numerical models. Mehdi et al. [32] investigated the relationship between a steam ejector's performance and cost criteria, where entrainment ratio and COP were used to reflect the performance, while the wall roughness is treated as cost. Similar concept was also adopted in the current study, where the cost is reflected by the increase in superheating, and exergy analysis is also included as a part of performance analysis. In real-life applications, droplets may exist during the ejector's operation. Daryoush et al. [33] investigated the relationship between decrease in ejector's efficiency and different wetness and number of droplets in secondary flow.

Despite many numerical studies that researchers have carried out, many failed to consider the steam's nonequilibrium condensation (NEC) effect. The NEC of steam occurs during the operation of the ejector, which involves high-speed flow expansions that leads to the state of steam exceeding the thermodynamic equilibrium

line due to the large gap between the inertial relaxation time and thermal relaxation time [34]. Steam at that point reaches high levels of supercooling. “Condensation shock” will occur as the state of steam abruptly revert to equilibrium [35]. The sharp change of the steam state is accompanied by instantaneous heat release as a large number of droplets form, and their latent heat is released. The drastic disturbance to the flow field will inevitably affect the accuracy of the ejector related studies. Nevertheless, the number of studies considering the NEC on ejector performances are still small compared to the studies using single-phase ideal gas or dry gas models. The reasons can be attributed to: (1). From an experimental perspective, as the flow speed inside an ejector is either transonic or supersonic, with the large amount of droplets condensed in a very short period, accurate measurement of the flow phenomenon is rather hard. Tang et al. [36] visualised the condensing jet flow experimentally, and condensing droplets were observed. Still, the detailed thermal dynamic analysis and complex flow structure are hard to be seen through the experiment. (2). From a numerical simulation perspective, computing the NEC effect can be computationally intensive, and the assumption of dry gas without condensation can also reflect some flow phenomena in an ejector; the potential error induced by NEC is often ignored. Ariafar et al. [37] studied the correlation between the mixing layer and entrainment ratio using the ideal gas assumption, neglecting the condensation behaviour. The results still indicated that compared to secondary flow pressure, the mixing layers have more impact on the entrainment ratio. Nevertheless, the impact of NEC has been noticed by researchers recently, and efforts were made to obtain more accurate results. Yang et al. [38] built an NEC model based on Young’s droplet growth model to investigate the performance of steam ejectors. The model captured the internal flow structures and the condensed phase parameters such as droplet radius. Mazzelli et al. [39] studied the NEC in steam ejectors by employing the SST k-ω turbulence model. Good alignment for mass flow rate and pressure were found between experiments and numerical studies.

With the previous research reviewed, the finding and novelty of the current study can be summarised as follows:

1) In this paper, an in-house two-phase condensing steam model is developed to study the performance of the steam ejector system for potential employment in battery thermal management systems utilising their cooling capacity.
2) The developed numerical model shows good capacity in capturing the complex NEC effect within a transonic process and various other flow behaviours inside the proposed steam ejector.
3) A low-temperature heat source provided by combustion waste heat from HEVs below 100°C is proposed and applied for the ejector battery thermal management system.
4) The ejector’s performance was investigated in various aspects, including entrainment ratio, coefficient of performance, and power, by tuning the primary flow’s superheating degree. An optimum point is found for the current setup.

The developed model is verified against existing experimental data inside both the Laval nozzle and steam ejector, and a good agreement was achieved. The different flow characteristics from the currently developed model and the commonly used dry gas assumption are revealed, and the condensing parameters were analysed in detail under different operating conditions. The findings from this study can be used for the design and operation of novel ejector driven HEV battery thermal management systems, which utilise low-grade combustion waste heat as the primary heat source.

In the future, the application of ejectors in other vehicles using renewable energies, such as fuel cell electric vehicles, can be explored as well because compared to HEVs, fuel cell electric vehicles may provide a constant heat flow rather than unsteady combustion waste heat.

2. Problem description

This study proposes a new approach for HEV battery thermal management systems by integrating the steam ejector refrigeration system into traditional battery systems. A working schematic and a skeleton p-h diagram of water showing the thermal dynamic process of the newly proposed ejector based battery thermal management system can be found in Figure 1. The critical points during the working process were labelled on the figure. A generator is used to provide the primary steam by recycling the engine waste heat. The secondary flow was sucked into the ejector at point 1 after cooling the battery. After mixing with the primary flow from the generator, the flow reaches point 2 before entering the condenser to be cooled down. The chilled water was then throttled to point 4 to cool the battery down in the battery thermal management system.

It should be noted that the currently proposed ejector cooling system should not be treated as the only solution for the battery thermal cooling system but rather as assistance or add-on to existing battery thermal

management systems. For application in Plug-in Hybrid Electric Vehicles (PHEV), the internal combustion engine will not work at all times; thus, their waste heat may not be sufficient to act as a single power source for the battery management system. Under these working conditions, the original battery management system utilising the vehicle's HVAC functions will still be available to ensure a safe working condition for the battery packs. Taking advantage of a numerical simulation, both the mass flow rate and the enthalpy at the points around the ejector can be extracted so that the ejector's power input and power output can be further calculated.

The basic working principle of the novel steam ejector enabled battery thermal management system is the same as a typical vehicle refrigeration system. The main difference between the two systems is: in the new thermal management system, the ejector plays the same role as the compressor in the traditional system, which usually consumes electricity as power input, while the ejector can effectively utilise the low-grade waste heat, saving part of the energy from external input. On the other hand, the moving parts inside the compressor make it costly for maintenance. At the same time, the ejector system is more robust and needs less maintenance. The heat pipe based battery thermal management component act as an evaporator compared to the traditional refrigeration system. Instead of just cooling down the vehicle cabin, the battery packs can also be cooled down using the same principle.

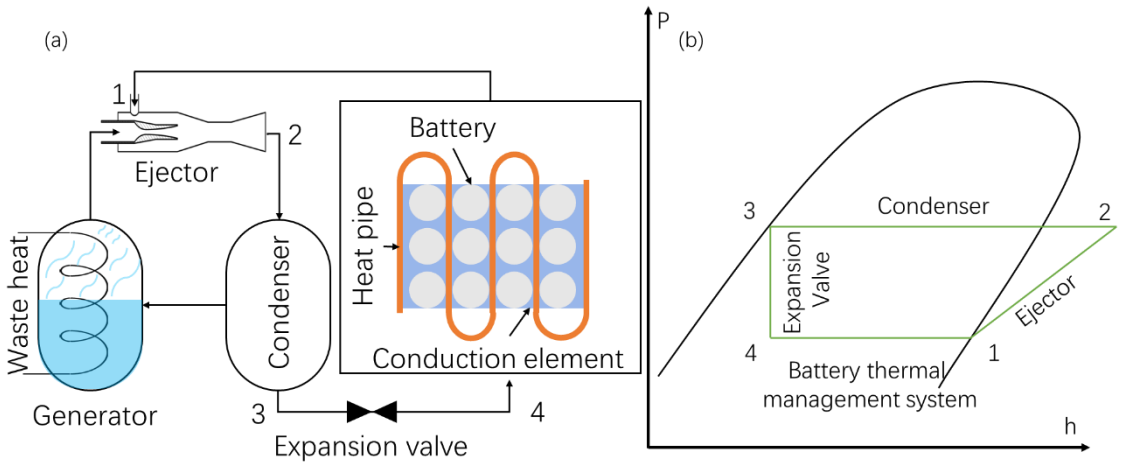

Figure 1 (a) Schematic of steam ejector based HEV battery thermal management system (b) p-h diagram showing the thermal dynamic process of the steam ejector based HEV battery thermal management system

A typical steam ejector configuration is shown in Figure 2. It is composed of the following parts: a primary nozzle, where motive steam flows through and expands to entrain the secondary low-pressure steam, from a suction chamber, where the two streams mix within a mixing chamber. The mixed flow then passes through a constant section and diffuser before being discharged to the condenser. The performance of a steam ejector is generally assessed by its coefficient of performance (COP), which is written as

$$COP = \frac{\dot{m}_s}{\dot{m}_p}\frac{(h_s - h_o)}{(h_p - h_o)} \tag{1}$$

where $\frac{\dot{m}_s}{\dot{m}_p}$ is the fraction between the mass flow rate of the secondary inlet (evaporator) and primary inlet (generator), which is also known as the entrainment ratio. h_o is the enthalpy of the outlet (condenser). From the equation, it can be seen that the COP is dependent mainly on the entrainment ratio. From this equation, it can also be seen that the entrainment ratio plays a critical role in determining the performance of an ejector.

In evaluation of thermodynamic performance of a ejector, exergetic efficiency can be utilized as a key indicator [40]. In the current study, exergy destruction from the ejector is analyzed with different operating conditions. The specific exergy can be defined as

$$e_x^* = h_{in}^* - h_0 - T_0(s_{in}^* - s_0) \tag{2}$$

Where the subscript 0 represents value at referencing temperature, in the current study, this temperature is taken as T_0 = 288K. h_{in}^* represnets enthalpy at primary and secondary inlet, depending on where the specific exergy should be calculated. Similarly, s_{in}^* represents entropy at the primary and secondary inlets. The exergy destruction e_{des} can then be calculated by

$$e_{des} = T_0 s_{gen} = T_0 \left(s_o - \frac{1}{1+\frac{\dot{m}_s}{\dot{m}_p}} s_p - \frac{\frac{\dot{m}_s}{\dot{m}_p}}{1+\frac{\dot{m}_s}{\dot{m}_p}} s_s \right) \quad (3)$$

Where s_{gen} is entropy generation, s_o, s_p, and s_s represents entropy of the outlet (condenser), primary inlet and secondary inlet, respectively.

With above concept defined properly, the exergy destruction ratio ψ_D for the ejector can then be calculated as

$$\psi_D = \frac{\left(1+\frac{\dot{m}_s}{\dot{m}_p}\right) e_{des}}{e_{x,p} + \frac{\dot{m}_s}{\dot{m}_p} e_{x,s}} \quad (4)$$

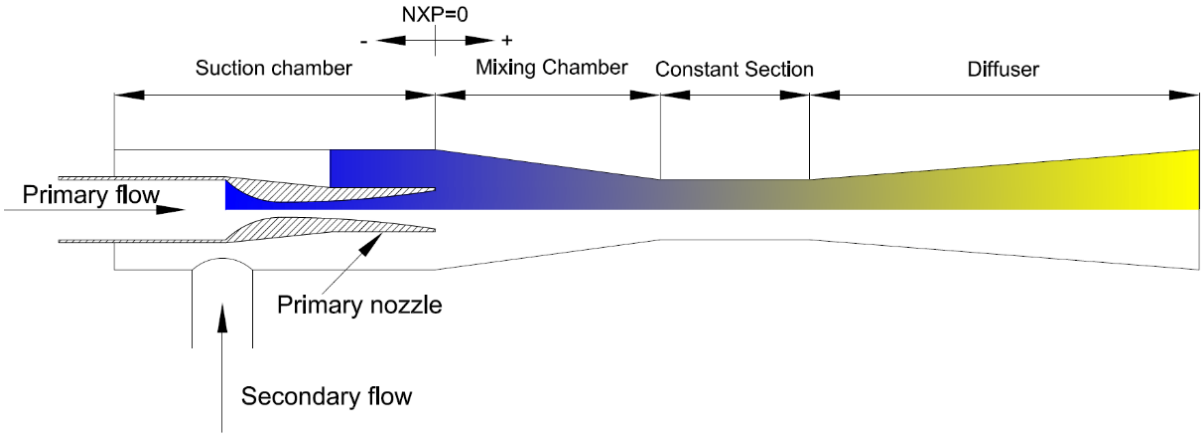

Figure 2 Steam ejector configuration. The coloured area indicates the 2D axisymmetric computational domain.

The performance curve for a steam ejector can be seen in Figure 3.

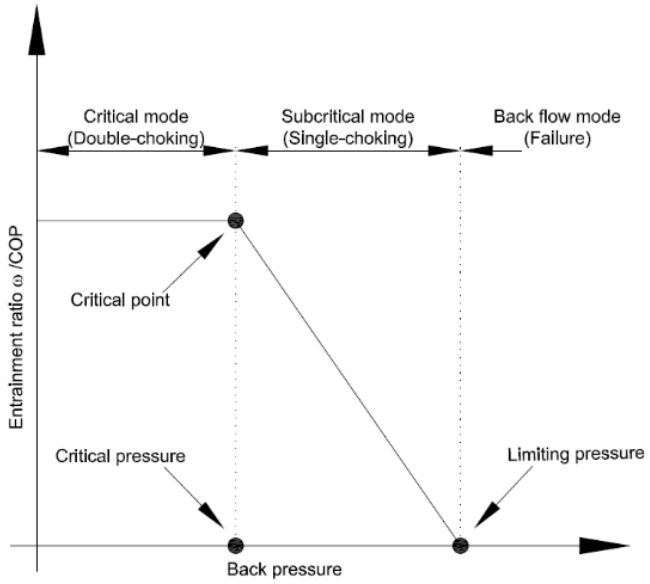

Figure 3 Performance curve of a typical steam ejector

Under the ideal working condition, primary flow with higher pressure serves as a driving force for the system by expanding in a converging-diverging nozzle, where a supersonic flow will occur, resulting in a vacuum region at the nozzle outlet, sucking secondary low pressure steam flow. The secondary steam flow sucked in will then be mixed with the primary flow in the mixing chamber, accelerated, and slowed down to near sonic inside the diffuser before being discharged to the outlet (condenser). The steam flow inside the primary nozzle will be chocked during this process, and the primary mass flow rate will reach the maximum. The secondary mass flow rate peaks during the acceleration process, where a second choking position emerges at the constant or diffuser section [41]. For a certain ejector, with the increase of backpressure, the second choking disappears, and the efficiency decreases drastically once the back pressure reaches beyond critical

pressure. Further increment of the backpressure beyond the limiting pressure will cause a backflow, and the ejector will fail.

3. Numerical model

At present, it is possible to model wet steam flow through build-in wet steam models in commercial CFD codes based on the Eulerian-Eulerian approach. Despite the ease of use, the limitation of such a model is also obvious as it is not possible to adjust model parameters to suit the problem better. To overcome this limitation, an in-house wet steam model has been developed under the framework of a widely employed commercial CFD code. The in-house model enabled more choices for both solver settings and possibilities of using various thermodynamic models.

3.1. Wet steam model

As water vapour is chosen as the working fluid in the current study, compressible Navier-Stokes equations are considered adequate to describe the NEC phenomena for transonic flow inside the steam ejector [42]. To describe the basic flow behaviour for the continuous mixture phase, conservation of mass, momentum, and energy are shown in Eqs (5) – (7) [43].

$$\frac{\partial \rho}{\partial t} + \frac{\partial \left(\rho u_j\right)}{\partial x_j} = -\dot{m} \tag{5}$$

$$\frac{\partial (\rho u_i)}{\partial t} + \frac{\partial \left(\rho u_j u_i\right)}{\partial x_j} = -\frac{\partial p}{\partial x_i} + \frac{\partial \tau_{ij}}{\partial x_j} - \dot{m} u_i \tag{6}$$

$$\frac{\partial (\rho E)}{\partial t} + \frac{\partial \left(\rho u_j E + p\right)}{\partial x_j} = -\frac{\partial \left(\lambda_{eff} \frac{\partial T}{\partial x_j}\right)}{\partial x_i} + \frac{\partial \left(u_i \tau_{ij}\right)}{\partial x_j} - \dot{m} h_{lv} \tag{7}$$

In Eq 4, τ_{ij} is the stress tensor, which can be expressed by

$$\tau_{ij} = \mu_{eff}\left(\frac{\partial u_i}{\partial x_j} + \frac{\partial u_j}{\partial x_i}\right) - \frac{2}{3}\mu_{eff}\frac{\partial u_k}{\partial x_k}\delta_{ij} \tag{8}$$

E is total energy, λ_{eff} is the effective thermal conductivity, μ_{eff} is the effective molecular dynamic viscosity, and h_{lv} is the enthalpy of a liquid droplet during evaporation [44, 45].

As for the source terms added to the above equations, the mass source term $\dot{m}$ represents the condensation rate of vapour, which can be expressed by

$$\dot{m} = \frac{4}{3} r^{*3} \rho_l J + 4\pi r^2 \rho_l N \frac{dr}{dt} \tag{9}$$

the first term on the right-hand side reflects the mass generation rate contributed by nucleation, while the second term reflects the mass generation rate contributed by droplet growth, where r^* is the critical droplet radius, expressed by

$$r^* = \frac{2\sigma}{\rho_l R T ln(S)} \tag{10}$$

where σ and ρ_l are liquid surface tension and condensate liquid density evaluated based on temperature separately, and S is supersaturation ratio, which is the ratio between vapour pressure and saturation pressure

$$S = \frac{p}{p_{sat}(T)} \tag{11}$$

The equation governing droplet growth modified by Hill [46] was utilised

$$\frac{dr}{dt} = \frac{P}{h_{lv}\rho_l\sqrt{2\pi RT}} \frac{\gamma + 1}{2\gamma} C_p (T_d - T) \tag{12}$$

Apart from the continuous phase, the calculation for properties of the condensed water droplet phase is realised by two additional transport equations shown in equations 13 and 14.

$$\frac{\partial (\rho Y)}{\partial t} + \frac{\partial \left(\rho u_j Y\right)}{\partial x_j} = \dot{m} \tag{13}$$

$$\frac{\partial (\rho N)}{\partial t} + \frac{\partial \left(\rho u_j N\right)}{\partial x_j} = \rho J \tag{14}$$

The effect of condensing phase on the continuous mixture phase is taken into account via the addition of source terms to the above-mentioned governing equations. ANSYS Fluent 19.2 was utilised as the computational platform to perform the calculations. The additional transport equations and source terms were realised using user-defined scalars (UDSs) and user-defined functions (UDFs).

In Eqs 13 and 14, two extra scalars Y and N are introduced, representing liquid mass fraction and droplet number per unit volume separately, and J is the droplet nucleation rate obtained from the classical nucleation theory [47, 48] expressed by

$$J = \frac{q_c}{1+\phi}\frac{\rho_v^2}{\rho_l}\sqrt{\frac{2\sigma}{\pi m_v^3}}\exp\left(-\frac{4\pi\sigma}{3k_BT}r^{*2}\right) \tag{15}$$

where m_v is the mass of a single molecule, k_B is Boltzmann's constant, ϕ is non-isothermal correction factor given by

$$\phi = \frac{2(\gamma-1)}{\gamma+1}\left(\frac{h_{lv}}{RT_v}\right)\left(\frac{h_{lv}}{RT}-0.5\right) \tag{16}$$

where γ is the ratio of specific heat capacities.

The following assumptions are made to cope with the model used: Firstly, the droplets formed via the spontaneous condensation process are small enough to not significantly affect the momentum of the carrying fluid. Thus, the condensed droplet phase shares the same velocity as the vapour phase. Secondly, the interaction between condensed droplets, including collision, breakup, and heat transfer, was neglected. Thirdly, the mixed flow temperature and pressure are the same as the vapour phase. Lastly, the relationship between mixture density and vapour density is expressed as

$$\rho_v = \rho(1-Y) \tag{17}$$

3.2. Turbulence modelling and numerical scheme

In this paper, the turbulence model chosen to predict the supersonic flow is $SST\ k-\omega$, as previous studies showed that a better capacity for predicting the flow behaviour against the experimental data is demonstrated compared to other turbulence models [49]. For $k-\omega$ model, k stands for turbulent kinetic energy, and ω stands for turbulence frequency. The govering equation for k and ω can be expressed as

$$\frac{\partial(\rho k)}{\partial t}+\frac{\partial(\rho k u_j)}{\partial x_j}=\frac{\partial\left[\left(\mu+\frac{\mu_t}{\sigma_k}\right)\frac{\partial k}{\partial x_j}\right]}{\partial x_j}+G_k-Y_k \tag{18}$$

$$\frac{\partial(\rho \omega)}{\partial t}+\frac{\partial(\rho \omega u_j)}{\partial x_j}=\frac{\partial\left[\left(\mu+\frac{\mu_t}{\sigma_\omega}\right)\frac{\partial \omega}{\partial x_j}\right]}{\partial x_j}+G_\omega-Y_\omega \tag{19}$$

Where G_k, Y_k, G_ω and Y_ω are rate of production and rate of dissipation of k and ω, σ_k and σ_ω are modeling constants. The coupled algorithm is used for pressure-velocity coupling. Transient simulation with a time step of 10^{-6} s is solved with double precision to capture the spontaneous condensation phenomena accurately. The convergence criterion for the relative residual of the continuity and all other dependent variables is set to 10^{-3} and 10^{-6}, respectively. The mass imbalance value is assigned as 10^{-4} to ensure iteration convergence. Total pressure and total temperature boundary conditions were assigned for the primary nozzle inlet and the secondary suction chamber inlet, while the diffuser exit employs the pressure outlet condition. In this simulation, the no-slip and adiabatic walls are assumed for the steam ejector.

4. Results & Discussion

4.1. Validation case study for nonequilibrium condensation model

Before applying the in-house condensation model directly to a steam ejector, its validity has to be examined in a simpler testing environment. In the current study, the validation case study is performed based on the Laval nozzle experiment carried out by Moses and Stein [50], where the pressure distribution and a series of droplet parameters were reported. Pressure inlet with the pressure of 40050 Pa and 374.30 K were adapted from the original experiment as the inlet boundary condition for the nozzle, and supersonic flow occurs at the outlet. However, the inlet pressure obtained after the current simulation reaches a stable condition is 38963.6 Pa, which is slightly lower than that measured in the original experiment. Both inlet pressures (P_0) obtained at the nozzle inlet from the experiment, and numerical study has been adapted for the validation purpose, and the results are shown in Figure 4. It can be observed that when the P_0 value obtained from numerical simulation is applied, the results agree very well with experimental data. However, if the P_0 value obtained from the original experiment is applied, a slight misalignment occurs for the pressure distribution. Apart from possible inaccuracy occurred in experimental measurements, another major reason for this difference can be attributed to the fact that condensing transonic flow is very sensitive to even small changes in its thermodynamic status. According to a study conducted by Jörg et al. [51], even 1K variation in temperature can cause a huge displacement between

the pressure distribution obtained by experimental and numerical means. Due to the sensitive nature of the condensing transonic flow and so many parameters affecting the flow dynamics, a detailed mechanism for this misalignment is still not available. Considering the above facts, the developed CFD model is convinced that it accurately reflected the NECs in supersonic flows.

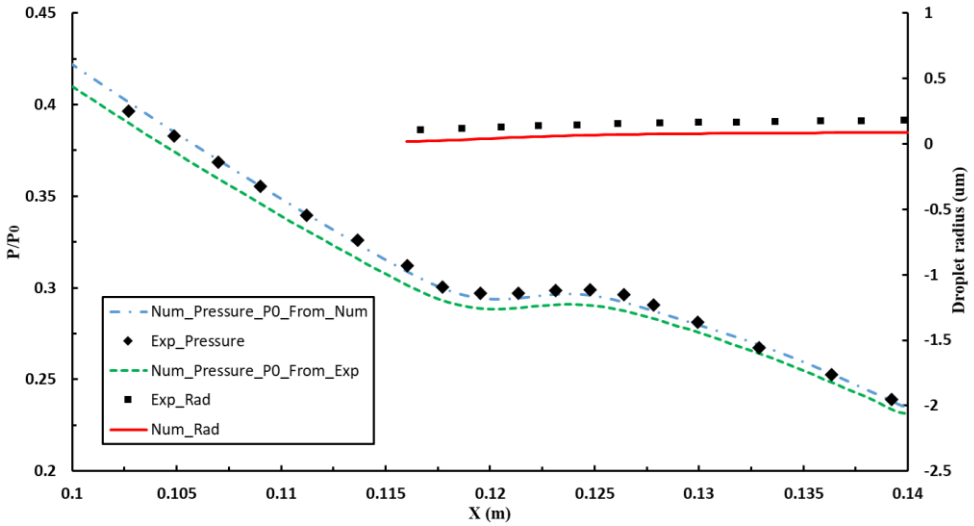

Figure 4 Numerical and experimental results at nozzle centreline.

4.2. Validation case study for steam ejectors

In this section, the developed model is validated against an experiment conducted by Al-Doori [52]. The operating condition at the primary inlet was 270 kPa, the pressure at the secondary (suction) inlet was 1.2 kPa, while the outlet pressure was 6 kPa. The primary nozzles' dimension was 10 mm, the throat diameter was 3.2 mm, and the nozzle outlet was 13.6 mm with 10° for the diverging angle. The ejector's outlet diameter was 50 mm. Detailed dimensions of the ejector can be obtained from the original literature.

Accurate prediction of the supersonic condensing flow behaviour inside the ejector relies heavily on the grid resolution. Based on this reason, to reduce diffusion caused by mesh during calculation, a structured mesh has been prepared for the current study. To better suit the $SST\ k-\omega$ model, mesh refinement has been applied near the wall boundaries to ensure the wall y+ value is below 1 for all mesh utilised. The mesh was generated using ANSYS Meshing. Before any formal calculation has been taken out, mesh sensitivity analysis is performed by comparing the liquid mass fraction along the centerline of the ejector. Three different mesh densities, namely coarse (140315 cells), medium (318860 cells) and fine (355050 cells), were tested using the same ejector geometry used in the original experiment, and the results are shown in Figure 5. The mesh sensitivity analysis indicates that the medium mesh density is utilised to carry out the current study to achieve a balance between accuracy and computational costs; thus, medium mesh density has been applied for both validation purposes and further analysis for the current study. The wall pressure measured during the experiment was compared with simulation results, and good agreement and consistency were shown in Figure 6 with error analysis using the root-mean-square (R^2) value. It is found that the developed numerical model is able to reflect the complicated flow behaviour inside a steam ejector with good accuracy. The detailed dimension of the ejector employed in the current study can be found in Table 1. The structure of the mesh employed in this study and the shape of the current ejector are shown in Figure 7.

Table 1 Dimensions of the ejector for the battery thermal management system.

Geometrical parameters	**Value**
Diameter of primary nozzle inlet	40 mm
Diameter of primary nozzle outlet	25.57 mm
Diameter of primary nozzle throat	10 mm
Length of primary nozzle	140 mm
Nozzle exit position	0 mm
Nozzle divergence angle	16°

Diameter of mixing section inlet	80 mm
Diameter of constant area	40 mm
Diameter of diffuser outlet	80 mm
Length of mixing section	150 mm
Length of constant area	100 mm
Length of diffuser	260 mm

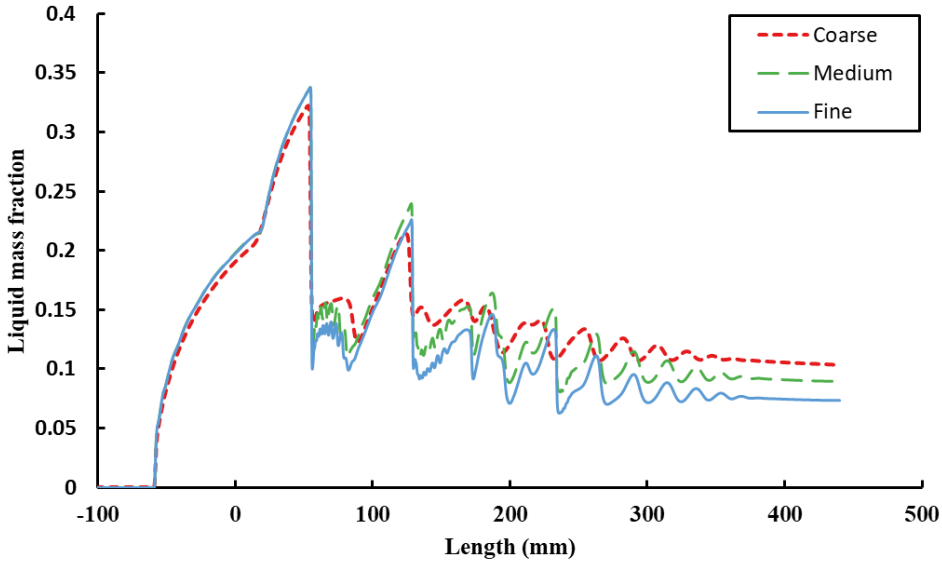

Figure 5 Liquid mass fraction inside the steam ejector under different mesh densities

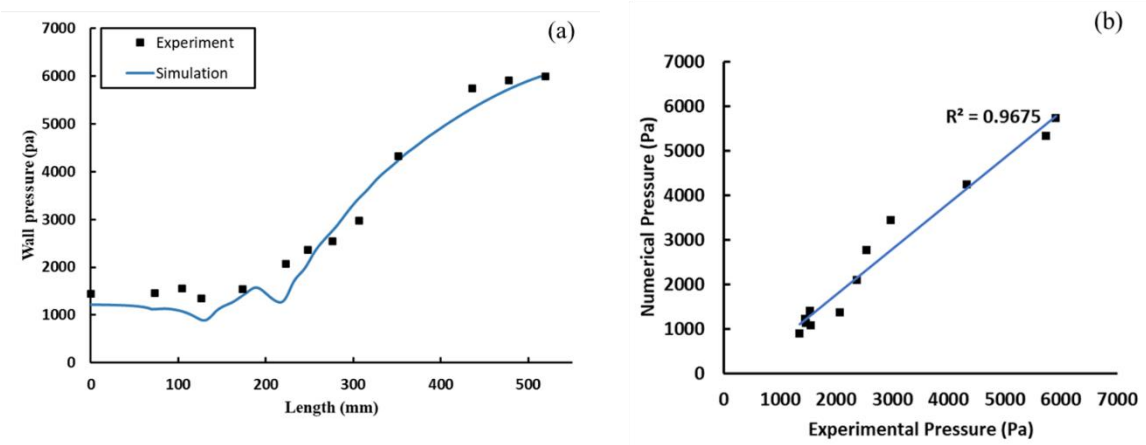

Figure 6 (a) comparison of wall pressure distribution for the ejector, (b) error analysis of pressure

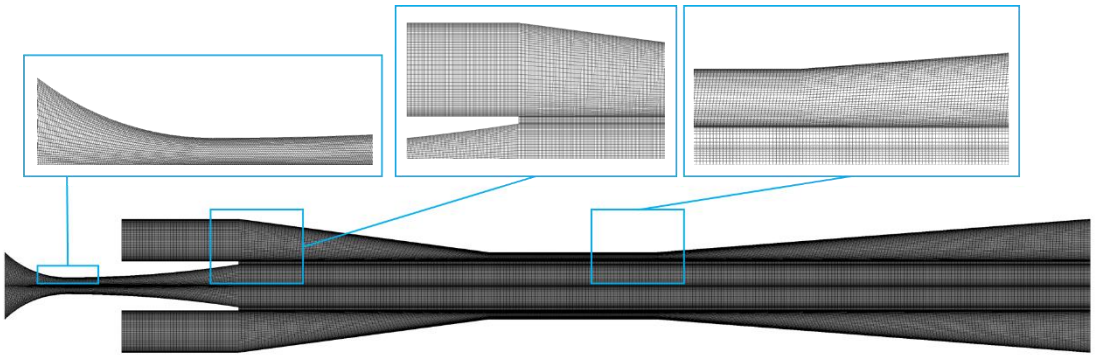

Figure 7 Mesh structure of the steam ejector for the battery thermal management system

4.3. A comprehensive investigation on flow behaviours

In this section, a series of comprehensive flow behaviour inside the steam ejector with spontaneous condensation phenomenon will be demonstrated with comparison to the ideal-gas model to showcase the effect of condensation using a baseline study. The performance of the ejector under different operating conditions was subsequently analysed using the entrainment ratio and COP as key indicators. Finally, some modification to the operating conditions to improve the ejector's performance was taken out, and relative recommendations were also made. The baseline case study employed saturated steam properties, with the pressure for the primary nozzle being 31.2 kPa, the pressure of the suction chamber inlet as 1.23 kPa, and the outlet back pressure being 2 kPa. Other parameters are also tested by modifying the base case study. A summary of boundary conditions used in the current study has been summarised in Table 2.

Table 2 Summary of boundary conditions used in the current ejector

Boundary conditions	**Inlet of primary nozzle**	**Inlet of suction chamber**	**Ejector outlet**					
Pressure (kPa)	31.2	1.23	2	2.25	2.5	2.75	3	3.25
Temperature (K)	343.15 (Saturated) 373.15 (30K superheating) 363.15 (20K superheating) 353.15 (10K superheating)	283.15	290.65	292.52	294.23	295.79	297.23	298.57
				N/A				

4.3.1. Comparison between the condensation model and dry gas assumption

The steam flow was accelerated inside the primary nozzle from sub-sonic to supersonic state. During the acceleration process, steam chokes at the nozzle throat and experiences a sharp expansion at the diverging region, where condensation appears with the steam passing through the saturation line. A low-pressure zone is formed near the exit of the primary nozzle. Thus fluids from the suction chamber can be sucked in and mixed in later parts of the ejector. Figs 8-14 compared the flow structures inside the ejector using different parameters with and without considering the condensation effect.

Mach number distribution inside the whole ejector and along the ejector centerline is depicted in Figure 8. It is seen that both models predicted similar trends, especially since the shock train was clearly captured from the nozzle exit plane to the diffuser. However, the difference between the results is also clear: the intensity of the Mach number inside the ejector is smaller when the condensation effect is taken into account. The peak Mach number for the ideal gas model case reaches around 3.47 near the exit of the primary nozzle, while the peak Mach number considering the condensation effect is only 2.55 at a similar location, and the peak also appears later along the axis. Apart from the peak, the intensity of the series of shock waves in the mixing section of the ejector is also higher when utilising the ideal gas assumption. The main reason for this difference can be attributed to the energy exchange due to condensation, as part of the energy of the steam flow is released during the phase change process, decreasing the momentum. This process is clearly reflected by the rapid drop of Mach number near the primary nozzle throat (X = 0), where the condensation happens.

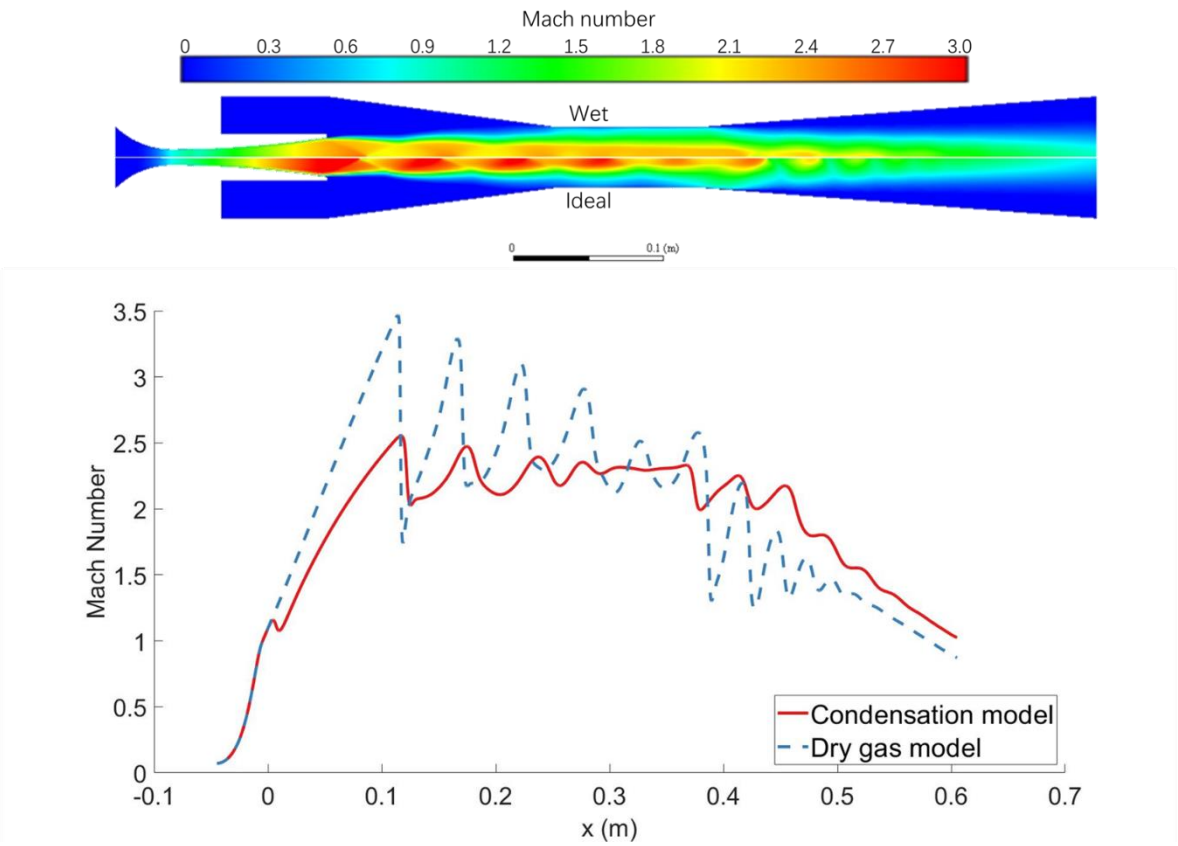

Figure 8 Mach number inside the steam ejector

Figure 9 shows the static pressure distribution inside the whole ejector and its distribution along the centerline. A series of alternating oblique shock and expansion waves were clearly observed using both models. This means that both models capture the under-expansion status of the steam in the primary nozzle. However, the pressure jump caused by condensation is only seen near the primary nozzle throat (X = 0) in Figure 9 with condensation taken into consideration. It is also seen that the fluctuation of pressure along the whole ejector is more intense when ignoring the condensation effect. The oblique shock waves appeared later compared to the dry gas assumption as well. It reveals the fact that during the condensation process, as droplets condense and subsequently grow, the heat and mass transfer between the gas phase and liquid phase takes part in the energy exchange for the whole steam flow, attenuating the pressure fluctuation and weakening the shock waves. The relatively more stable pressure distribution inside the ejector also reflected a stable and complete mixing process.

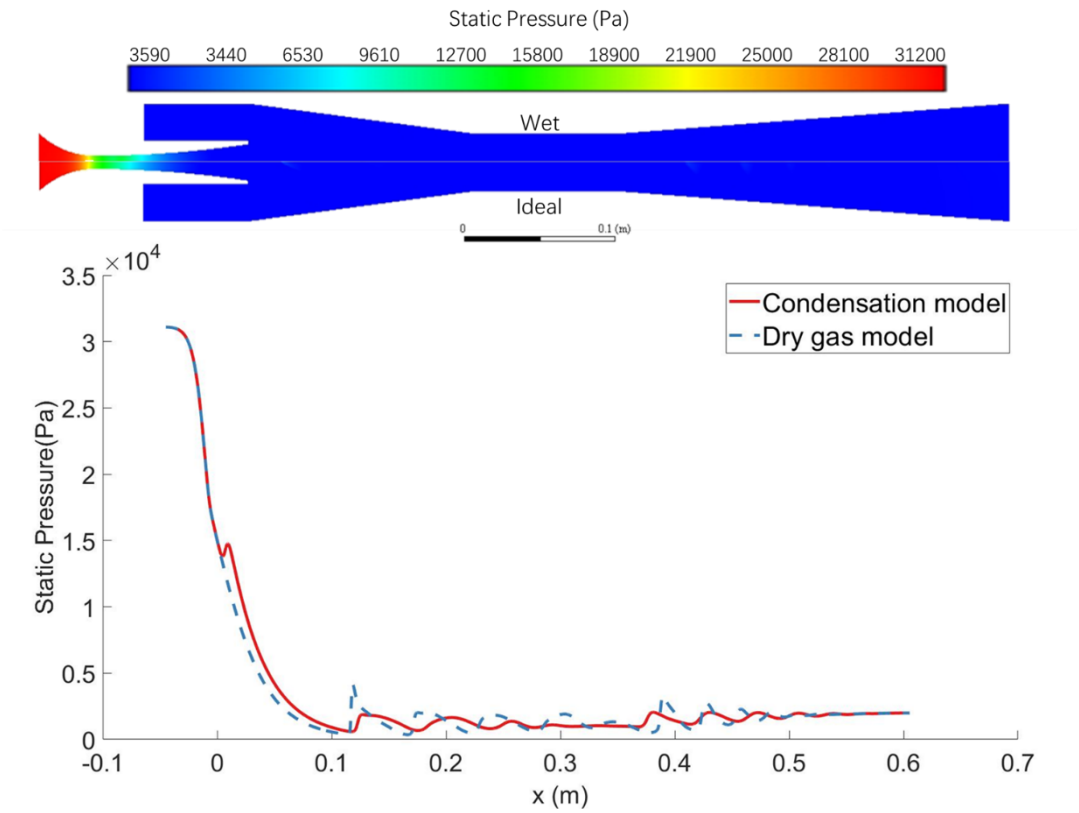

Figure 9 Static pressure inside the steam ejector

Temperature distribution through the whole ejector and along the ejector centerline was shown in Figure 10. The latent heat release during intense spontaneous condensation is intuitively reflected through the temperature change. A sharp jump in temperature near where the condensation happens (X = 0). It is also observed that without consideration of condensation, the dry gas assumption will lead to unphysical values in temperature, where the lowest temperature inside the ejector reaches as low as 115 K, where icing should have taken place, and the ejector will fail. On the other side, the temperature remains physically valid inside the ejector once the latent heat released during a phase change is involved in the calculation.

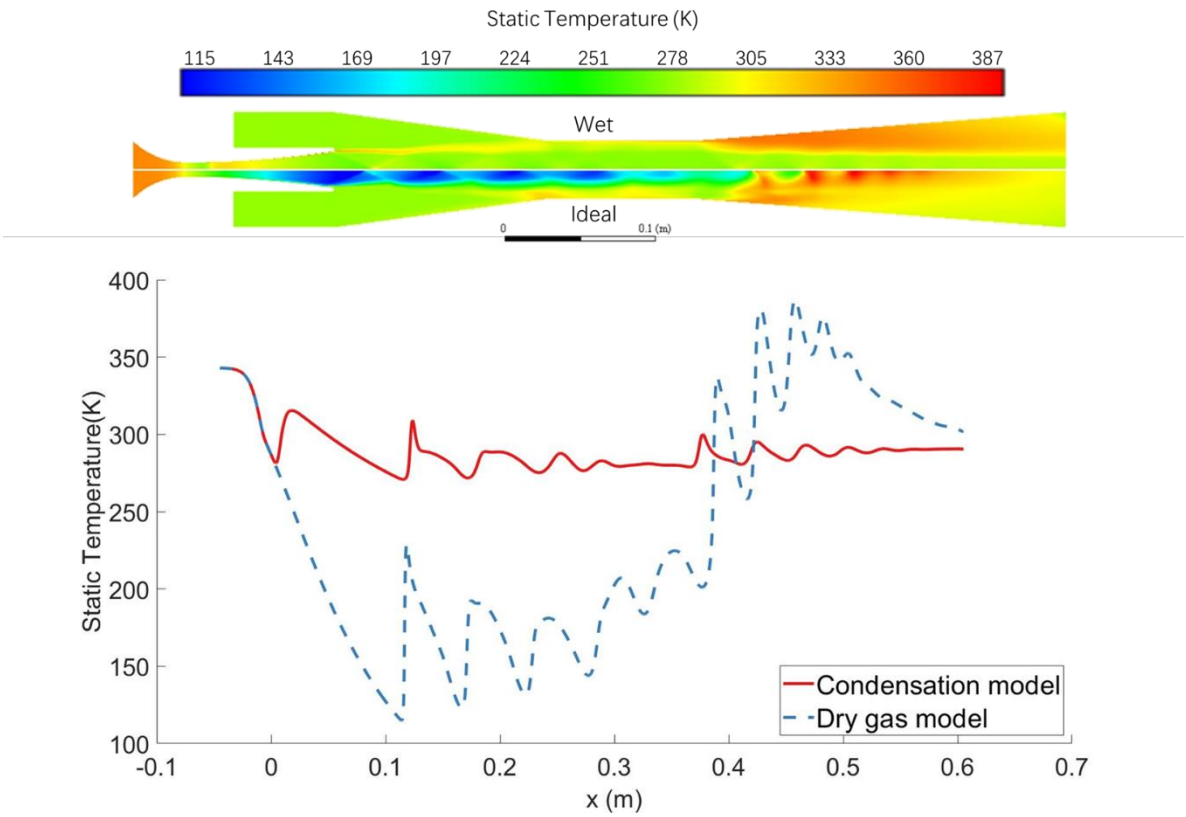

Figure 10 Static temperature inside the steam ejector

All these differences in flow behaviours show that ignoring the condensation phenomena will result in a large disparity in the physical phenomena, leading to an inaccurate or even unphysical evaluation of the ejector performance. On the other hand, the current wet steam model can also be improved using the Lagrangian method to bypass the assumptions made for the current model and obtain more detailed information about the condensing droplets [53].

4.3.2. Characteristics of condensing flow

Condensation features will be further illustrated in this section, including the nucleation rate, supersaturation ratio and liquid mass fraction.

The droplet nucleation rate can be analysed in conjunction with the steam supersaturation ratio. The nucleation rate reflects the intensity of spontaneous condensation, while the steam supersaturation ratio determines the possibility of nucleation. The droplet nucleation rate and supersaturation ratio through the whole ejector and along the ejector centerline were shown in Figure 11 and Figure 12, respectively. It can be seen that the nucleation process took place only in a very short region near the primary nozzle throat (X = 0), and both the increasing and decreasing trend of the nucleation rate happens sharply, indicating the spontaneous nature of this condensation process. Compared with the supersaturation ratio, it is seen that the nucleation starts as soon as the supersaturation exceeds unity, with the physical meaning of the steam status passed through the saturation line to the supersaturated region. The intensity of nucleation reaches its peak at maximum supersaturation and subsequently decreases with the retrieval of equilibrium, where the supersaturation ratio drops below unity.

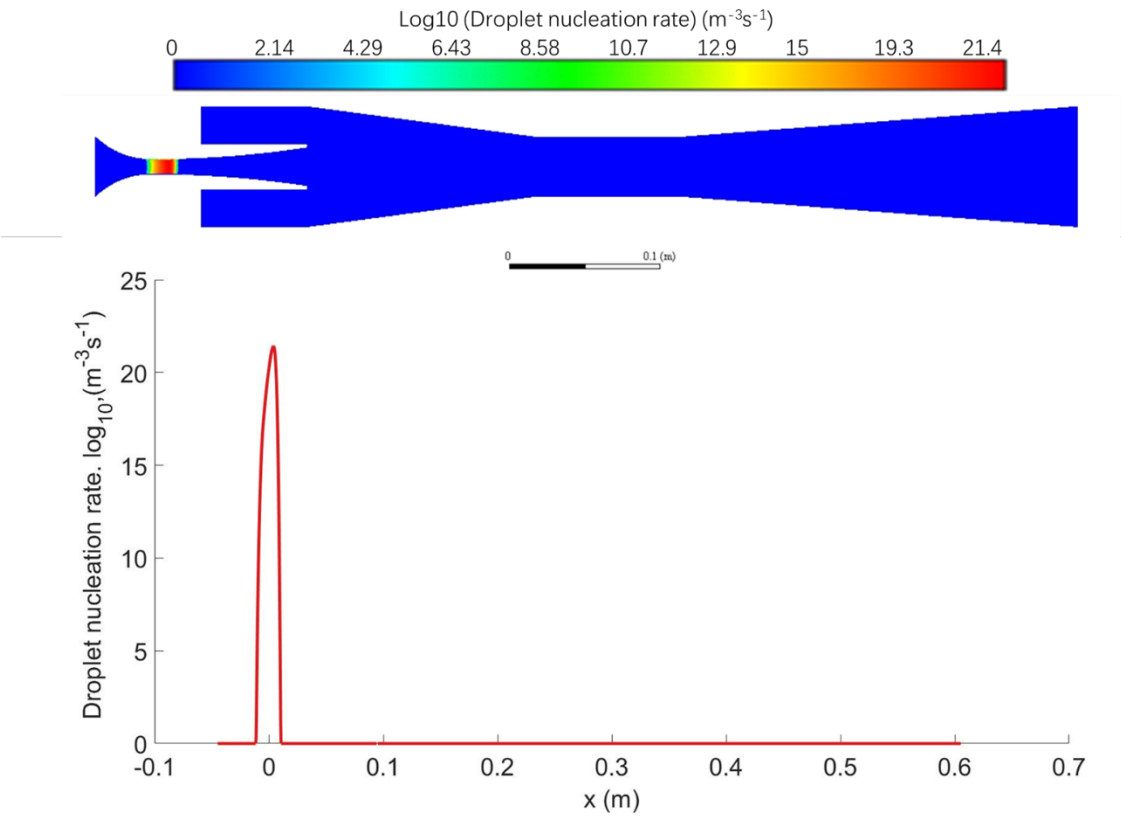

Figure 11 Droplet nucleation rate inside the steam ejector

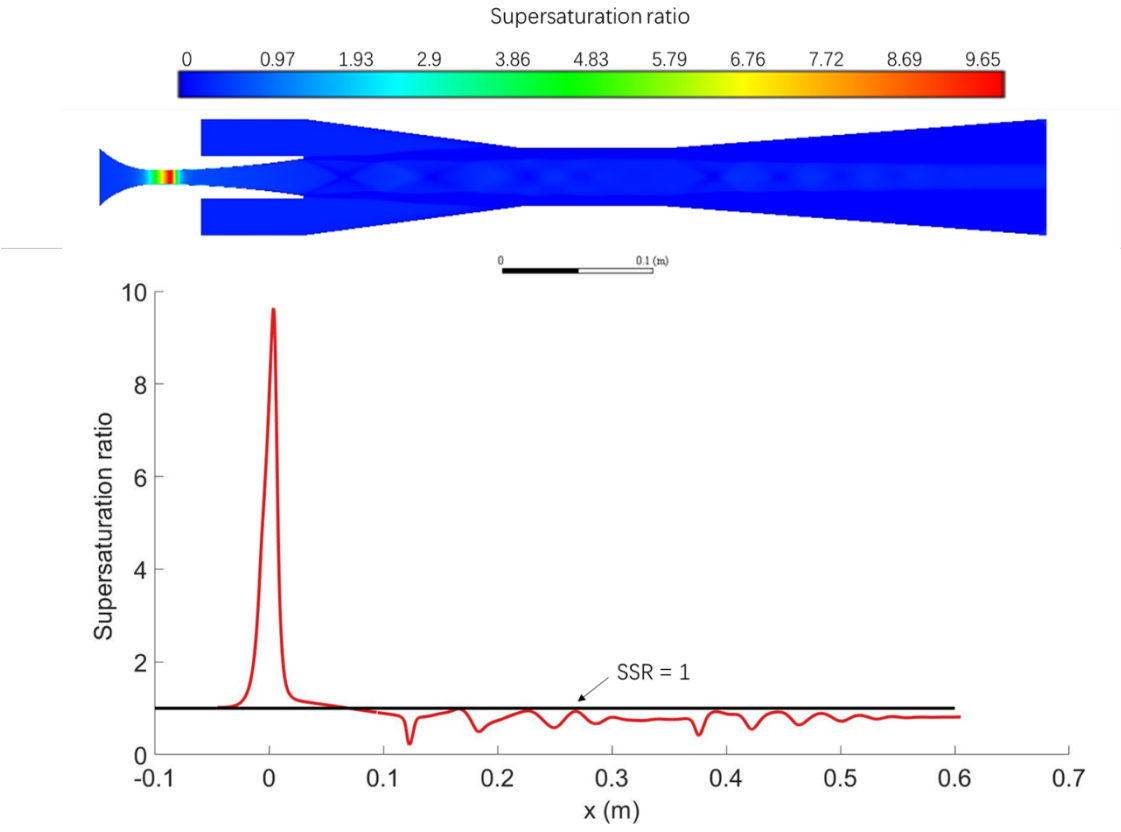

Figure 12 Steam supersaturation ratio inside the steam ejector

The spontaneous nucleation near the primary nozzle throat contributed to the first rapid increment of the liquid mass fraction to its peak at 0.162, as seen in Figure 13. The droplet growth happened intensely at the nucleation front and rapidly decreased to a much lower level. It can be seen that the liquid mass fraction subsequently decreased and fluctuated, which is due to the continuous process of moisture building up on existing droplets as well as droplets re-evaporating, reflected by the droplet growth rate fluctuating with both positive and negative values along with the ejector, following the same pattern as the expansion waves, revealed in Figure 14.

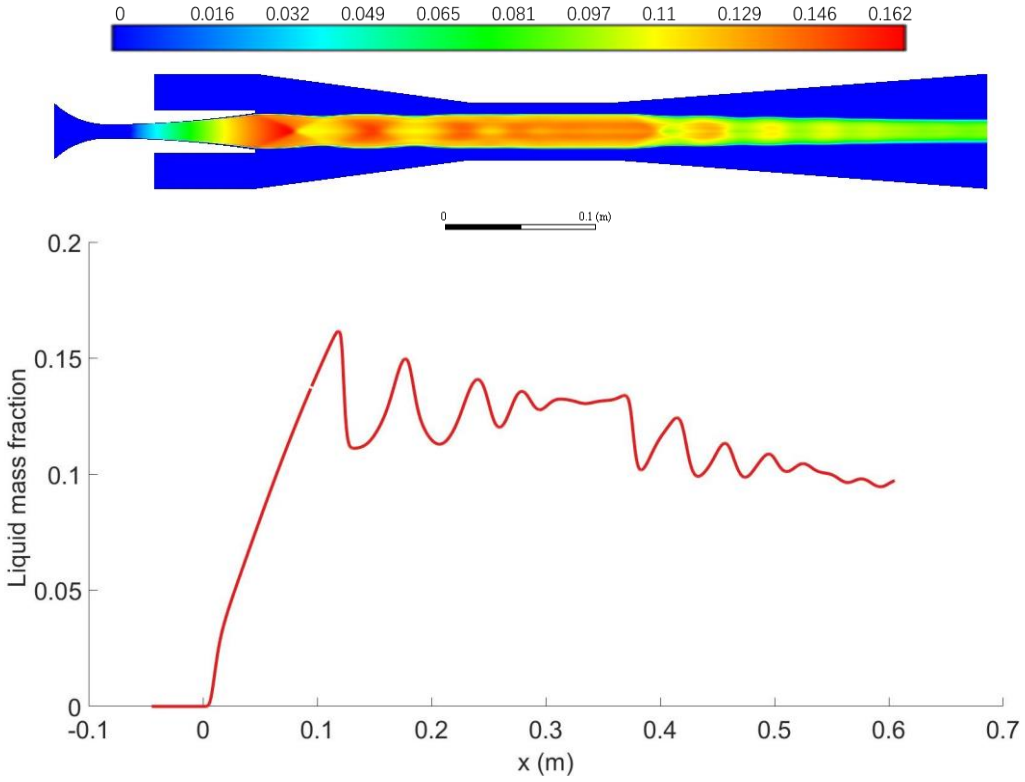

Figure 13 Liquid mass fraction inside the steam ejector

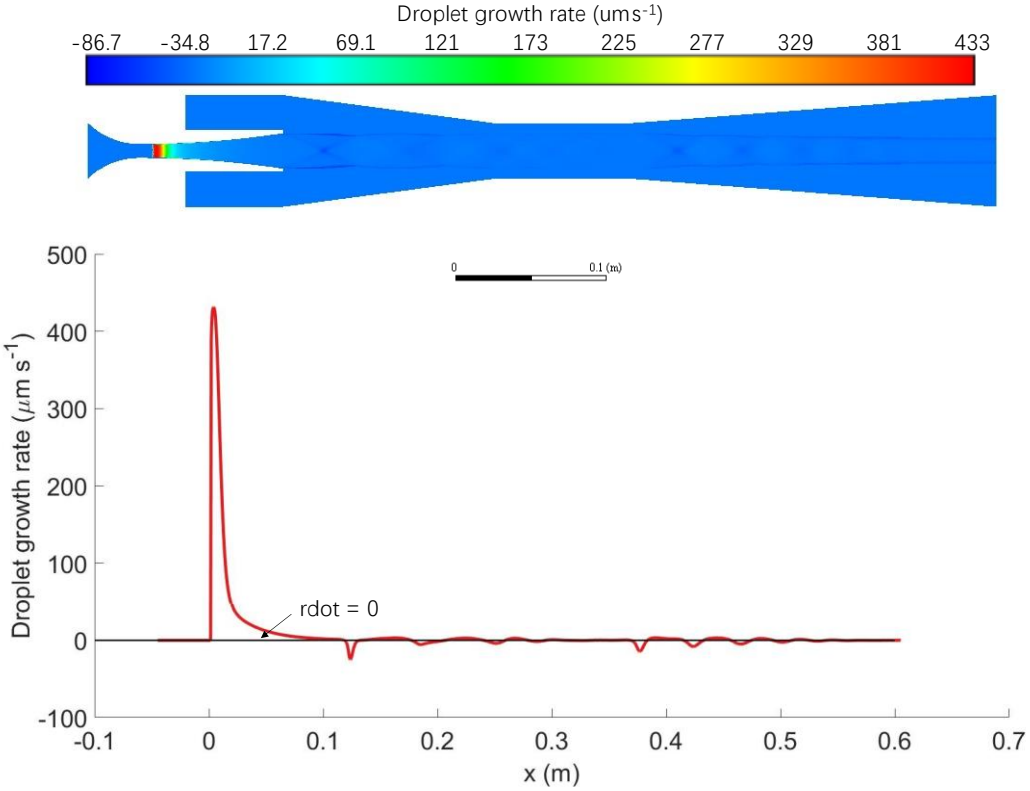

Figure 14 Droplet growth rate inside the steam ejector

4.4. Performance evaluation for an ejector for HEV battery thermal management system

With essential condensing flow behaviours captured with the inclusion of condensation into the calculation, the evaluation of ejector performance can then be carried out by comparing the entrainment ratio and COP. The ejector's efficiency in the sense of power utilisation is also analysed by comparing their intake power and output power.

In the current study, different back pressures were first employed to evaluate the primary performance and capacity of the current ejector. Figure 15 illustrates the performance curve of the current ejector under different operating back pressures, with and without consideration of the spontaneous condensation effect. When the back pressure reaches 3.25 kPa, the entrainment ratio becomes negative, indicating a failed ejector. Since the negative entrainment ratio is meaningless, it is thus shown as 0 on the chart to indicate the failed working condition. For the baseline case study with 2 kPa back pressure, the entrainment ratio predicted by both models is similar. In contrast, with the increase of backpressure, the relative error between the two models increases. However, the difference in COP reflects the error in the first place. It can also be seen that the ejector performance is underestimated using the dry gas assumption.

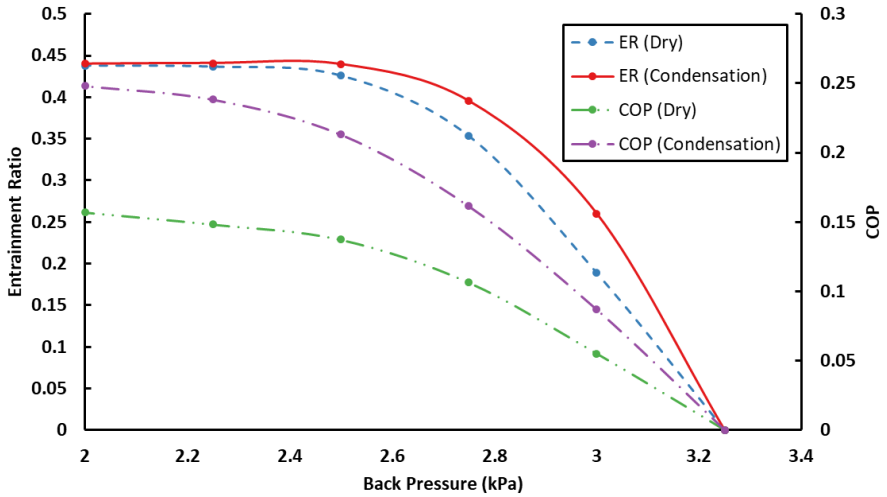

Figure 15 Performance curves of the steam ejector with different backpressure using different models

With the aim of improving the performance of the current ejector, superheating of primary flow as a novel approach is proposed. To evaluate the effect of the superheating of the primary nozzle inlet temperature on the ejector performance, the single variable method is adopted for the baseline case where 2 kPa backpressure is adopted. With the suction pressure and temperature remaining unchanged, the primary nozzle inlet temperature gradually increases with the original saturation pressure, so that the variation of entrainment ratio is only contributed by superheating of primary flow. The effect of the primary steam superheating on the entrainment ratio calculated by the model considering the condensation effect is shown in Figure 16.

From the results, it can be seen that: 1) With the increment of superheating degree for primary steam, the entrainment ratio of the current ejector increases, which indicates that increasing the superheating degree can enhance the entrainment of secondary steam. It can be attributed to the effect of enhanced NEC brought by larger superheating, which elongated the time for steam to return to equilibrium. 2) Although more secondary steam can be entrained from a low-pressure suction chamber, the COP of the ejector itself decreases as the superheating degree increases. This is because increasing the superheating degree will require more energy input, thus deducting the COP of the whole ejector. It is also found that an optimum point exists at the crossing point of the entrainment ratio line and COP line when the superheating degree is around 11 K for the current setup. At this point, the entrainment ratio increased by 2% compared with no superheating, while the COP decreased by around 9%.

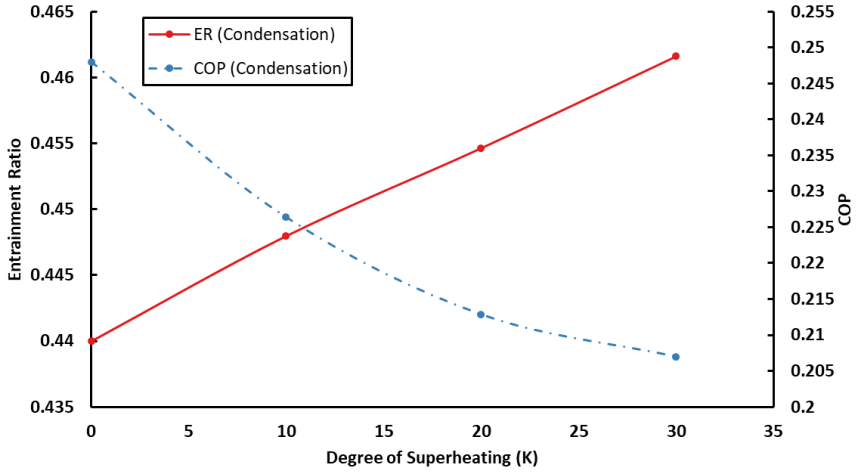

Figure 16 The influence of the primary inlet superheating degree on the ejector's performance

The role of an ejector in the whole ejector battery thermal management system is analogue to that of an electrical compressor in a regular refrigeration system; the power intake and output of the ejector can be compared under different operating scenarios. For the ejectors, the power intake is from the primary flow; after sucking the secondary flow in with the complex mixing process, the flow is compressed and directed to the

condenser, which is the power output. The power intake and output, the ejector's efficiency as a compressor, the exergy destruction and exergy destruction ratio of the ejector have been summarised in Table 3. It can be seen that the ejector's performance as a compressor is subject to the backpressure, which agrees with the conclusion from previous results regarding the entrainment ratio and COP. In the baseline case, the ejector's efficiency as a compressor can reach 36%, with this portion of energy all contributed from the primary steam flow, which essentially comes from the collected waste heat. With the increment of the primary flow's superheating degree, the power output of the ejector increases as well, but the efficiency of the current ejector as a compressor remains unchanged. It is thus desirable to increase the degree of superheating to the primary flow to enhance the ejector's output capacity while not sacrificing its efficiency. Combined with previous findings, under the current setup, a superheating degree of 11K to the primary flow is optimum. Although further increasing the inlet superheating degree helps to enhance the ejector's entrainment performance, it will also significantly decrease its COP. For example, with 30K superheating, the entertainment ratio increased by 5%, but the COP decreased by 17%. In terms of exergy analysis, comparing the exergy destruction and exergy destruction ratio, it is seen that with increase of superheating degree, both the exergy destruction and exergy destruction ratio decreases, reflecting on an improved exergetic efficiency. The exergy destruction and exergy destruction ratio of the current ejector is lower compared to a compressor [54].

Table 3 Ejector's power performance under different working conditions

Degree of superheating (K)		Backpressure (kPa)	Q_output (W)	Q_input (W)	Efficiency	Exergy destruction (kW)	Exergy destruction ratio ψ_D
Saturated	0	2	119.8	337.1	36%	200.74	0.0796
		2.25	113.3	337.1	34%	184.19	0.0730
		2.5	97.2	337.1	29%	167.91	0.0666
		2.75	68.0	337.1	20%	158.68	0.0627
		3	28.8	337.1	9%	168.21	0.0656
Superheated	10	2	139.2	406.7	34%	192.11	0.0762
	20	2	160.1	474.7	34%	184.13	0.0730
	30	2	184.0	541.0	34%	177.01	0.0701

5. Conclusions

This study investigated an ejector-based cooling system for battery thermal management systems within HEVs driven by low temperature, low-grade waste energy from combustion waste heat at around 70 °C. Comparisons between the dry gas model and the developed wet-steam approach indicated the failed capacity of the dry gas model on flow structure, the reflection of physical behaviours, and the evaluation of ejector systems' performances. The dry gas model will give unphysical predictions without considering the condensation effect (i.e., 115 K for the dry gas model, while the condensation model presents temperature at 271 K, the deviation is up to 136%). The dry gas assumption also underestimates the entrainment ratio and coefficient of performance of the steam ejector. In contrast, the current model successfully captured the spontaneous condensation effect and its related heat and mass transfer process. By considering the physical behaviours occurring within the enclosure, the flow field and performance of the proposed ejector can be accurately evaluated. It can be concluded that the complex phase change phenomena within a supersonic ejector should be modelled to obtain a more accurate reflection of the system.

As a baseline study, with a back pressure of 2 kPa and primary steam temperature at 70 °C, the entrainment ratio for the proposed ejector was found as 0.44. Increasing the primary flow's superheating degree was proposed for working cycle optimisation. The increment of superheating degrees to 30 K increases the entrainment ratio to 0.46 with a reduction in COP. With regards to the power intake and output, it was observed that increasing the degree of superheating for the primary flow increased the power output by 54% without sacrificing the ejector's efficiency. Overall, by balancing the entrainment ratio, COP, and performance in power, optimal performance has been achieved for this system. In essence, this superheating degree is around 11 K, where a 2% increase in entrainment ratio was obtained without further decreases in COP. In summary, numerical simulations can be performed to study steam ejectors' effectiveness on HEV's thermal management system, with the benefits of recycling low-grade combustion waste heat that enhances the overall energy efficiency and eco-friendliness.

Acknowledgements: This research includes computations using the computational cluster Katana supported by Research Technology Services at UNSW Sydney. This research was sponsored by the Australian Research Council (ARC Industrial Transformation Training Centre IC170100032).

Data Availability Statement: The research data supporting this publication are provided within this paper.

Conflicts of Interest: The authors declare no conflict of interest.

References

[1] S. Küfeoğlu, D. Khah Kok Hong, Emissions performance of electric vehicles: A case study from the United Kingdom, Applied Energy, 260 (2020).

[2] J. Du, D. Ouyang, Progress of Chinese electric vehicles industrialization in 2015: A review, Applied Energy, 188 (2017) 529-546.

[3] Y. Qiu, F. Jiang, A review on passive and active strategies of enhancing the safety of lithium-ion batteries, International Journal of Heat and Mass Transfer, 184 (2022).

[4] P. Sun, R. Bisschop, H. Niu, X. Huang, A Review of Battery Fires in Electric Vehicles, Fire Technology, 56(4) (2020) 1361-1410.

[5] B. Mao, C. Zhao, H. Chen, Q. Wang, J. Sun, Experimental and modeling analysis of jet flow and fire dynamics of 18650-type lithium-ion battery, Applied Energy, 281 (2021).

[6] F. Zhang, X. Feng, C. Xu, F. Jiang, M. Ouyang, Thermal runaway front in failure propagation of long-shape lithium-ion battery, International Journal of Heat and Mass Transfer, 182 (2022).

[7] A.M. Bizeray, S. Zhao, S.R. Duncan, D.A. Howey, Lithium-ion battery thermal-electrochemical model-based state estimation using orthogonal collocation and a modified extended Kalman filter, Journal of Power Sources, 296 (2015) 400-412.

[8] Y. Ma, X. Li, G. Li, Y. Hu, Q. Bai, SOC Oriented Electrochemical-Thermal Coupled Modeling for Lithium-Ion Battery, IEEE Access, 7 (2019) 156136-156149.

[9] Y. Zhou, H.-x. Li, S. Xie, Fast Modeling of Battery Thermal Dynamics Based on Spatio-temporal Adaptation, IEEE Transactions on Industrial Informatics, (2021) 1-1.

[10] Y.R. Zhi, B. Yu, A.C.Y. Yuen, J. Liang, L.Q. Wang, W. Yang, H.D. Lu, G.H. Yeoh, Surface Manipulation of Thermal-Exfoliated Hexagonal Boron Nitride with Polyaniline for Improving Thermal Stability and Fire Safety Performance of Polymeric Materials, ACS Omega, 3(11) (2018) 14942-14952.

[11] M. Ghiji, V. Novozhilov, K. Moinuddin, P. Joseph, I. Burch, B. Suendermann, G. Gamble, A Review of Lithium-Ion Battery Fire Suppression, Energies, 13(19) (2020).

[12] H. Zhou, F. Zhou, L. Xu, J. Kong, QingxinYang, Thermal performance of cylindrical Lithium-ion battery thermal management system based on air distribution pipe, International Journal of Heat and Mass Transfer, 131 (2019) 984-998.

[13] S. Gungor, E. Cetkin, S. Lorente, Canopy-to-canopy liquid cooling for the thermal management of lithium-ion batteries, a constructal approach, International Journal of Heat and Mass Transfer, 182 (2022).

[14] K.V. Jithin, P.K. Rajesh, Numerical analysis of single-phase liquid immersion cooling for lithium-ion battery thermal management using different dielectric fluids, International Journal of Heat and Mass Transfer, 188 (2022).

[15] J. Li, A. Tang, X. Shao, Y. Jin, W. Chen, D. Xia, Experimental evaluation of heat conduction enhancement and lithium-ion battery cooling performance based on h-BN-based composite phase change materials, International Journal of Heat and Mass Transfer, 186 (2022).

[16] M.M. El Idi, M. Karkri, M. Abdou Tankari, A passive thermal management system of Li-ion batteries using PCM composites: Experimental and numerical investigations, International Journal of Heat and Mass Transfer, 169 (2021).
[17] Y. Gan, L. He, J. Liang, M. Tan, T. Xiong, Y. Li, A numerical study on the performance of a thermal management system for a battery pack with cylindrical cells based on heat pipes, Applied Thermal Engineering, 179 (2020).
[18] J. Wang, Y. Gan, J. Liang, M. Tan, Y. Li, Sensitivity analysis of factors influencing a heat pipe-based thermal management system for a battery module with cylindrical cells, Applied Thermal Engineering, 151 (2019) 475-485.
[19] K. Sumeru, L. Martin, F.N. Ani, H. Nasution, F.N. Ani, Energy Savings in Air Conditioning System Using Ejector: An Overview, Applied Mechanics and Materials, 493 (2014) 93-98.
[20] D. Butrymowicz, J. Gagan, M. Łukaszuk, K. Śmierciew, A. Pawluczuk, T. Zieliński, M. Kędzierski, Experimental validation of new approach for waste heat recovery from combustion engine for cooling and heating demands from combustion engine for maritime applications, Journal of Cleaner Production, 290 (2021).
[21] M. Karvonen, R. Kapoor, A. Uusitalo, V. Ojanen, Technology competition in the internal combustion engine waste heat recovery: a patent landscape analysis, Journal of Cleaner Production, 112 (2016) 3735-3743.
[22] R. Zhang, W. Su, X. Lin, N. Zhou, L. Zhao, Thermodynamic analysis and parametric optimization of a novel S–CO2 power cycle for the waste heat recovery of internal combustion engines, Energy, 209 (2020).
[23] M.d.A. Al-Nimr, A.A. Alajlouni, Internal combustion engine waste heat recovery by a thermoelectric generator inserted at combustion chamber walls, International Journal of Energy Research, 42(15) (2018) 4853-4865.
[24] J. Yan, W. Cai, Y. Li, Geometry parameters effect for air-cooled ejector cooling systems with R134a refrigerant, Renewable Energy, 46 (2012) 155-163.
[25] A. Selvaraju, A. Mani, Experimental investigation on R134a vapour ejector refrigeration system, International Journal of Refrigeration, 29(7) (2006) 1160-1166.
[26] Z. Bo, L.W.W. Mihardjo, M. Dahari, A.G. Abo-Khalil, A.-R. Al-Qawasmi, A.M. Mohamed, T. Parikhani, Thermodynamic and exergoeconomic analyses and optimization of an auxiliary tri-generation system for a ship utilizing exhaust gases from its engine, Journal of Cleaner Production, 287 (2021).
[27] J. Dong, X. Chen, W. Wang, C. Kang, H. Ma, An experimental investigation of steam ejector refrigeration system powered by extra low temperature heat source, International Communications in Heat and Mass Transfer, 81 (2017) 250-256.
[28] Y. Han, L. Guo, X. Wang, A.C.Y. Yuen, C. Li, R. Cao, H. Liu, T.B.Y. Chen, J. Tu, G.H. Yeoh, A Steam Ejector Refrigeration System Powered by Engine Combustion Waste Heat: Part 1. Characterization of the Internal Flow Structure, Applied Sciences, 9(20) (2019).
[29] Y. Han, X. Wang, L. Guo, A.C.Y. Yuen, H. Liu, R. Cao, C. Wang, C. Li, J. Tu, G.H. Yeoh, A Steam Ejector Refrigeration System Powered by Engine Combustion Waste Heat: Part 2. Understanding the Nature of the Shock Wave Structure, Applied Sciences, 9(20) (2019).
[30] X. Wang, J. Dong, A. Li, H. Lei, J. Tu, Numerical study of primary steam superheating effects on steam ejector flow and its pumping performance, Energy, 78 (2014) 205-211.
[31] G. Zhang, S. Dykas, M. Majkut, K. Smołka, X. Cai, Experimental and numerical research on the effect of the inlet steam superheat degree on the spontaneous condensation in the IWSEP nozzle, International Journal of Heat and Mass Transfer, 165 (2021).

[32] M.P. Rad, E. Lakzian, A. Grönman, Numerical investigation of roughness effect on wet steam ejector performance in the refrigeration cycle, Heat and Mass Transfer, (2022).
[33] D. Dadpour, E. Lakzian, M. Gholizadeh, H. Ding, X. Han, Numerical modeling of droplets injection in the secondary flow of the wet steam ejector in the refrigeration cycle, International Journal of Refrigeration, 136 (2022) 103-113.
[34] G. Zhang, X. Zhang, D. Wang, Z. Jin, X. Qin, Performance evaluation and operation optimization of the steam ejector based on modified model, Applied Thermal Engineering, 163 (2019).
[35] C. Wen, N. Karvounis, J.H. Walther, H. Ding, Y. Yang, Non-equilibrium condensation of water vapour in supersonic flows with shock waves, International Journal of Heat and Mass Transfer, 149 (2020).
[36] Y. Tang, Z. Liu, Y. Li, H. Wu, X. Zhang, N. Yang, Visualization experimental study of the condensing flow regime in the transonic mixing process of desalination-oriented steam ejector, Energy Conversion and Management, 197 (2019) 111849.
[37] K. Ariafar, D. Buttsworth, G. Al-Doori, N. Sharifi, Mixing layer effects on the entrainment ratio in steam ejectors through ideal gas computational simulations, Energy, 95 (2016) 380-392.
[38] Y. Yang, X. Zhu, Y. Yan, H. Ding, C. Wen, Performance of supersonic steam ejectors considering the nonequilibrium condensation phenomenon for efficient energy utilisation, Applied Energy, 242 (2019) 157-167.
[39] F. Mazzelli, F. Giacomelli, A. Milazzo, CFD modeling of condensing steam ejectors: Comparison with an experimental test-case, International Journal of Thermal Sciences, 127 (2018) 7-18.
[40] H. Ding, Y. Zhao, C. Wen, C. Wang, C. Sun, Energy efficiency and exergy destruction of supersonic steam ejector based on nonequilibrium condensation model, Applied Thermal Engineering, 189 (2021).
[41] Y. Han, X. Wang, H. Sun, G. Zhang, L. Guo, J. Tu, CFD simulation on the boundary layer separation in the steam ejector and its influence on the pumping performance, Energy, 167 (2019) 469-483.
[42] C. Wen, B. Rogie, M.R. Kærn, E. Rothuizen, A first study of the potential of integrating an ejector in hydrogen fuelling stations for fuelling high pressure hydrogen vehicles, Applied Energy, 260 (2020).
[43] C. Wen, H. Ding, Y. Yang, Performance of steam ejector with nonequilibrium condensation for multi-effect distillation with thermal vapour compression (MED-TVC) seawater desalination system, Desalination, 489 (2020).
[44] A.G. Gerber, M.J. Kermani, A pressure based Eulerian–Eulerian multi-phase model for non-equilibrium condensation in transonic steam flow, International Journal of Heat and Mass Transfer, 47(10-11) (2004) 2217-2231.
[45] H. Liu, I.M. De Cachinho Cordeiro, A.C.Y. Yuen, C. Wang, A. Li, G.H. Yeoh, Numerical modeling of wet steam infused fluid mixture for potential fire suppression applications, Experimental and Computational Multiphase Flow, (2021).
[46] P.G. Hill, Condensation of water vapour during supersonic expansion in nozzles, Journal of Fluid Mechanics, 25(3) (2006) 593-620.
[47] J.B. Young, Two-Dimensional, Nonequilibrium, Wet-Steam Calculations for Nozzles and Turbine Cascades, Journal of Turbomachinery, 114(3) (1992) 569-579.
[48] C. Wen, H. Ding, Y. Yang, Numerical simulation of nanodroplet generation of water vapour in high-pressure supersonic flows for the potential of clean natural gas dehydration, Energy Conversion and Management, 231 (2021) 113853.

[49] Y. Han, X. Wang, A.C.Y. Yuen, A. Li, L. Guo, G.H. Yeoh, J. Tu, Characterization of choking flow behaviors inside steam ejectors based on the ejector refrigeration system, International Journal of Refrigeration, 113 (2020) 296-307.

[50] C.A. Moses, G.D. Stein, On the growth of steam droplets formed in a Laval nozzle using both static pressure and light scattering measurements, Journal of Fluids Engineering, 100(3) (1978) 311-322.

[51] J. Starzmann, F.R. Hughes, A.J. White, M. Grübel, D.M. Vogt, Numerical Investigation of Boundary Layers in Wet Steam Nozzles, Journal of Engineering for Gas Turbines and Power, 139(1) (2017).

[52] G.F.L. Al-Doori, Investigation of refrigeration system steam ejector performance through experiments and computational simulations, 2013.

[53] T. Wittmann, C. Bode, J. Friedrichs, The Feasibility of an Euler–Lagrange Approach for the Modeling of Wet Steam, Journal of Engineering for Gas Turbines and Power, 143(4) (2021).

[54] S. Agarwal, A. Arora, B.B. Arora, Energy and exergy analysis of vapor compression–triple effect absorption cascade refrigeration system, Engineering Science and Technology, an International Journal, 23(3) (2020) 625-641.